Revista Ciencia en Desarrollo. Vol. 16 Num. 2. pp. 115 - 122
julio - diciembre

DOI: 10.19053/uptc.01217488.v16.n2.2025.18900

Artículo de investigación

Proposal of a computational method for the detection of asbestos-cement in hyperspectral images based on spectral signature binarization and Hamming distance

Propuesta de método computacional para la detección de asbesto-cemento en imágenes hiperespectrales a partir de la binarización de la firma espectral y la distancia de Hamming

Gabriel Elías Chanchí-Golondrino[1]✉, Manuel Alejandro Ospina-Alarcón[1]✉ y Manuel Saba[1]✉

[1]Facultad de Ingeniería de la Universidad de Cartagena, Colombia.

Recepción: 26-febrero-2025 **Aceptado:** 30-abril-2025 **Publicado:** 20-julio-2025
Cómo citar: Chanchí Golondrino, G. E., Ospina Alarcón, M. A., & Saba, M. (2025). Propuesta de método computacional para la detección de asbesto-cemento en imágenes hiperespectrales a partir de la binarización de la firma espectral y la distancia de Hamming. Caso de estudio: Barrio Manga de la ciudad de Cartagena. *Ciencia En Desarrollo*, 16(2). doi:10.19053/uptc.01217488.v16.n2.2025.18900

Abstract

One of the challenges in the field of hyperspectral imaging is the development of computationally effective and efficient methods for material detection given the large volume of data in these images. Based on this, this article proposes a computational method for detecting asbestos-cement as a contribution, using the binarization of the spectral signature of asbestos and its comparison with the binarized spectral signatures of the image pixels through the normalized Hamming distance. As a result of this research, the method was implemented using open-source libraries (spectral, numpy, matplotlib, and pandas) and was applied as a case study to a hyperspectral image of the Manga neighborhood in the city of Cartagena. The proposed method. The effectiveness and efficiency of the proposed method were compared with the correlation method, showing that the proposed method has similar effectiveness to the correlation method and is 4.92% more efficient. Based on the obtained results, the proposed method is a competitive alternative for replication and extrapolation in the detection of different materials in hyperspectral images. Likewise, given its efficiency results, this method can be integrated into material monitoring systems based on remote sensing.

Keywords: Asbestos detection, Hamming distance, hyperspectral images, remote sensing.

Resumen

Uno de los desafíos en el campo de las imágenes hiperespectrales es contar con métodos eficaces y eficientes computacionalmente que permitan la detección de materiales ante el gran volumen de datos de estas imágenes. A partir de lo anterior, en este artículo se propone como contribución un método computacional para la detección de asbesto-cemento, a partir de la binarización de la firma espectral de asbesto y su comparación con las firmas espectrales binarizadas de los píxeles de la imagen mediante la distancia normalizada de Hamming. Como resultado de esta investigación, se implementó el método mediante el uso de las librerías de código abierto (spectral, numpy, matplotlib y pandas) y se desplegó a modo de caso de estudio sobre una imagen hiperespectral del barrio Manga de la ciudad de Cartagena. El método propuesto. La eficacia y la eficiencia del método propuesto fueron comparadas con respecto al método de correlación, obteniendo que el método propuesto tiene una eficacia similar al método de la correlación y es 4.92% más eficiente. A partir de los resultados obtenidos, el método propuesto es una alternativa competitiva para ser replicado y extrapolado en la detección de diferentes materiales en imágenes hiperespectrales. Así mismo, dado los resultados a nivel de eficiencia, este método puede ser integrado en sistemas de monitorización de materiales basados en sensado remoto.

Palabras Clave: Detección de asbesto, distancia de Hamming, imágenes hiperespectrales, sensado remoto.

E-ISSN: 2462-7658

1 Introduction

Remote sensing involves the observation of the Earth's surface from space or air and can be defined as a technology that enables the measurement and analysis of objects or phenomena without direct contact with them, utilizing the detection of electromagnetic radiation reflected or emitted by objects, which is captured by sensors that may be located on platforms such as satellites, drones, or aircraft [1, 2, 3, 4]. Compared to traditional methods, remote sensing offers advantages such as temporal efficiency, cost-effectiveness, and the ability to collect data beyond the visual range [5].

One of the most widely used remote sensing methods is hyperspectral imaging, which integrates spectroscopy into conventional images to obtain three-dimensional data known as "datacubes," incorporating two spatial dimensions (x, y) and one spectral dimension (λ) [6, 7, 8]. In this way, each pixel in the datacube includes a complete spectrum that represents the absorption and scattering properties of light in the sampled spatial area [7, 9]. In this sense, given that each material has a representative spectral signature, this signature enables the classification of different types of land cover materials, such as vegetation, rocks, water bodies, and artificial structures, even when they appear visually similar [10, 11].

Several studies have been conducted for the detection of asbestos-cement in hyperspectral images. Thus, in [12, 13, 14], hyperspectral images in the shortwave infrared (SWIR: 1000–2500 nm) range have been used for the detection and classification of asbestos minerals, such as amosite, crocidolite, and chrysotile, where these identifications are based on the unique spectral signatures of each mineral, which are related to hydroxyl absorption bands. On the other hand, in [14, 15], hyperspectral images have been used to identify asbestos-containing materials in construction and demolition waste, enabling the separation of non-hazardous materials through multivariate analysis methods such as principal component analysis and partial least squares discriminant analysis. Likewise, in [16], hyperspectral images have been utilized in asbestos mine restoration projects to assess the distribution of this material before and after remediation, demonstrating high accuracy in detecting treated and untreated areas.

Now, regarding the challenges of hyperspectral images, it is important to mention that they contain a large amount of data due to their high dimensionality, which complicates data processing and analysis due to redundancy in the spectral band information [17, 18]. For this reason, in the domain of hyperspectral imaging, it is necessary to employ computationally efficient processing and analysis techniques [19, 20]. Likewise, it is important to highlight that traditional algorithms for analyzing these images are often computationally intensive, which limits their applicability for real-time analysis and in systems with limited resources [21, 22]. Given these challenges, it is essential to develop methods that are computationally efficient while providing results as effective as those of traditional methods for material detection in hyperspectral images.

In this article, a new computational method is proposed as a contribution for the detection of asbestos-cement in hyperspectral images, based on the binarization of the spectral signature of this material and the application of the normalized Hamming distance between the binarized signature and the binarized signatures of the other pixels. It is worth mentioning that, for the binarization process, the binarization threshold that allows the best differentiation was determined by evaluating the method with different thresholds on a sample of spectral signatures of asbestos and other materials. Based on the optimal binarization threshold determined, a case study was developed in which the proposed method was applied to a hyperspectral image of the Manga neighborhood in the city of Cartagena de Indias, aiming to identify asbestos-cement areas and quantify their corresponding percentage within the image. This is particularly useful for governmental authorities in formulating asbestos mitigation strategies, considering the implications for respiratory diseases among individuals exposed to this material [31, 32, 33]. Similarly, the proposed method was evaluated in terms of effectiveness and computational efficiency compared to the correlation method, which is one of the most widely used approaches for material detection in the context of hyperspectral imaging [23, 24]. For the implementation of the method, advantages provided by open-source technologies within the Python programming language were leveraged, including the spectral library for accessing and managing hyperspectral data, as well as the numpy library for implementing binarization and the Hamming distance. In this sense, the proposed method is accessible for replication or extrapolation in the detection of asbestos-cement and other materials in the domain of hyperspectral imaging [25, 26, 27].

The present study contributes significantly on two key fronts. First, from a public health perspective, early detection of asbestos-containing materials is crucial to mitigate the risks associated with prolonged exposure. Accurate identification of asbestos-cement coverings in urban environments allows for more effective monitoring and remediation strategies, contributing to environmental and health policy decisions. Thus, from the computational point of view, this work introduces an innovative methodology based on spectral signature binarization and Hamming distance comparison. This approach allows the detection of the material using a significantly reduced amount of information with respect to the original spectral signature, which represents an advantage in terms of computational efficiency and handling of the high dimensionality inherent to hyperspectral images.

The remainder of the article is organized as follows: Section 2 presents the methodological phases employed for the development of this research. Section 3 describes the obtained results, which include the determination of binarized signals of the asbestos spectral signature based on different thresholds associated with the mean and various statistical quantiles; the evaluation of the different binarized signals using sample spectral signatures of asbestos and other materials to determine the optimal quantile that allows the creation of the binarized signal with the best detection capability; the implementation of the method on the reference hyperspectral image corresponding to the Manga neighborhood in the city of Cartagena; and the evaluation of the effectiveness and efficiency of the proposed method compared to the correlation method. Finally, Section 4 presents the conclusions and

future work derived from this research.

2 Materials and methods

For the development of this research, four methodological phases were defined (see Figure 1): P1. Selection of sample pixels corresponding to asbestos and other materials, P2. Determination of the characteristic spectral signature of asbestos from the sample pixels, P3. Determination of the optimal binarization threshold based on the sample pixels and the characteristic spectral signature, and P4. Evaluation of the effectiveness and efficiency of the method in a case study.

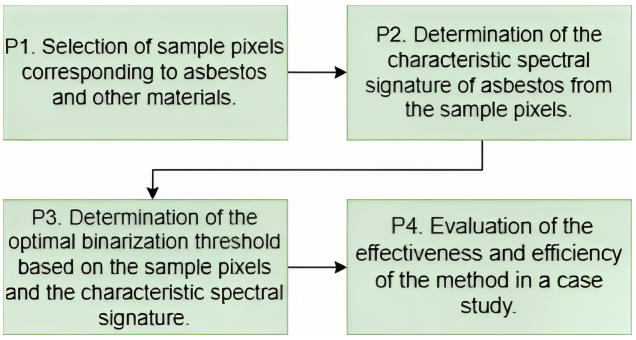

Figure 1: Considered methodology.

In Phase 1 of the methodology, a set of 75 asbestos pixels and 75 pixels of other materials were selected through visual inspection from the RGB representation of a hyperspectral image of 725x850 pixels, each containing a total of 380 reflectance bands. In this way, in Figure 2, it is possible to observe the RGB representation of the hyperspectral image of the Manga neighborhood in the city of Cartagena, where the 75 sample pixels of asbestos-cement are highlighted in blue, and the 75 sample pixels of other materials are highlighted in red.

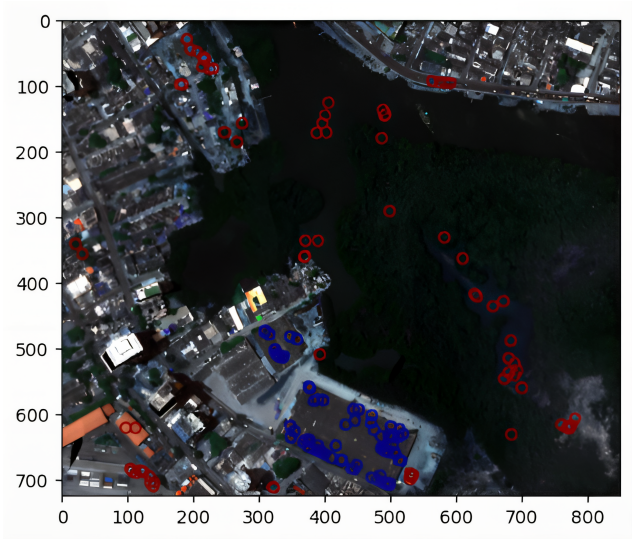

Figure 2: Sample pixels selected from asbestos and other materials.

In this same sense, in Phase 2 of the methodology, the characteristic pixel of asbestos-cement was determined by computing the mean of the 380 bands from the asbestos sample pixels selected in Phase 1. Thus, in Figure 3, the spectral signature of the asbestos-cement sample pixels is presented along with the average pixel, or characteristic pixel, obtained.

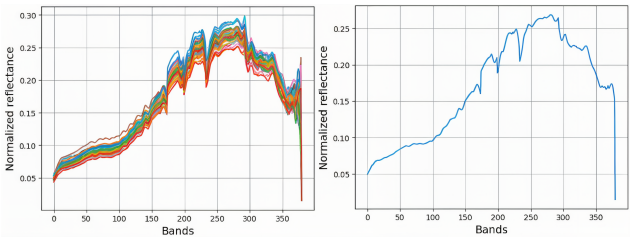

Figure 3: Asbestos-cement characteristic spectral signature.

Similarly, in Phase 3 of the methodology, different binarization thresholds were evaluated using the asbestos and non-asbestos sample pixels to determine the threshold that provides the best differentiation of asbestos-cement pixels. For threshold variation, the values associated with the 100 percentage quantiles of the spectral signature were considered. Thus, for each threshold value, the binarized signature of the average pixel was obtained, and the similarity percentage was calculated based on the normalized Hamming distance between this signature and the binarized signatures of each of the 150 sample pixels of asbestos and other materials, aiming to determine the maximum difference between the minimum similarity percentage with asbestos pixels and the maximum similarity percentage with pixels of other materials. In this sense, for the calculation of the binarized signature of the average pixel and other pixels, Equation (1) was used, where the filter with threshold T is applied to the normalized reflectance array of 380 positions $R = [r_1, r_2, \ldots, r_{380}]$, yielding the binarized array B_i as the result.

$$B_i = \begin{cases} 1, & \text{if } r_i \geq T \\ 0, & \text{if } r_i < T \end{cases} \tag{1}$$

Similarly, to obtain the similarity between the binarized array corresponding to the average pixel and the binarized arrays of the other pixels, Equation (2) was used, which represents the normalized Hamming distance between two binarized arrays, A and B. It is worth mentioning that, in this case, n corresponds to the total number of bands in the hyperspectral image.

$$d_H(A, B) = \frac{1}{n} \sum_{i=1}^{n} 1(a_i \neq b_i) \tag{2}$$

On the other hand, in Phase 4 of the methodology, a case study was conducted using the hyperspectral image corresponding to the Manga neighborhood in the city of Cartagena. The proposed method was applied to the entire image, and the percentage of asbestos-cement within the image was obtained. This percentage was compared to the percentage of asbestos-cement detected in the same image using the correlation method, which has been widely used for material

detection in hyperspectral images. Finally, within this phase, a 20×20 pixel region of the image, containing 380 bands, was selected for the execution of both the proposed method and the correlation method at 25, 50, 75, and 100 repetitions to determine the average execution time and the total average time for each method. In this way, based on the total average time of each method, the relative computational efficiency of the proposed method was determined.

3 Results and discussion

At the results level, the first step was to obtain the binarized spectral signature of the average asbestos pixel, using the median value of the spectral signature as the threshold (threshold = 0.171). In this way, Figure 4 presents the binarized spectral signature of asbestos-cement based on the mentioned threshold.

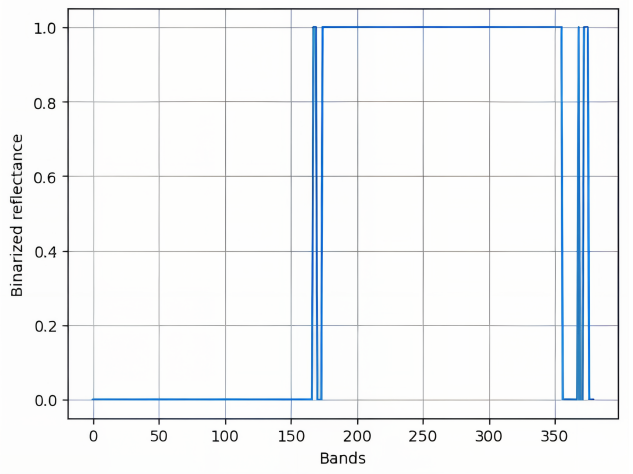

Figure 4: Asbestos-cement binarized spectral signature.

In this way, in Figure 4, it can be observed how the binarized spectral signature of asbestos oscillates between 0 and 1 across different bands. Initially, the signal remains at 0 in the first bands, indicating low reflectance in those wavelengths. Subsequently, around band 150, the signal abruptly shifts to 1, maintaining this value until approximately band 320, suggesting a high reflectance range. Finally, in the last bands, the signal exhibits fluctuations between 0 and 1, reflecting variations in the absorption and scattering properties of the material in those spectral regions.

Using the binarized spectral signature of asbestos-cement presented in Figure 4, the similarity was calculated based on the normalized Hamming distance between this signature and the signatures of the 75 asbestos pixels and the 75 pixels of other materials, obtaining the minimum and maximum normalized distances for each group of pixels, as shown in Figure 5.

From Figure 5, it is possible to observe that the maximum percentage-normalized Hamming distance with non-asbestos pixels (99.947%) exceeds the minimum normalized distance with asbestos pixels (99.908%), indicating the presence of overlap. Consequently, the threshold value set at the median does not allow the method based on the binarization of the

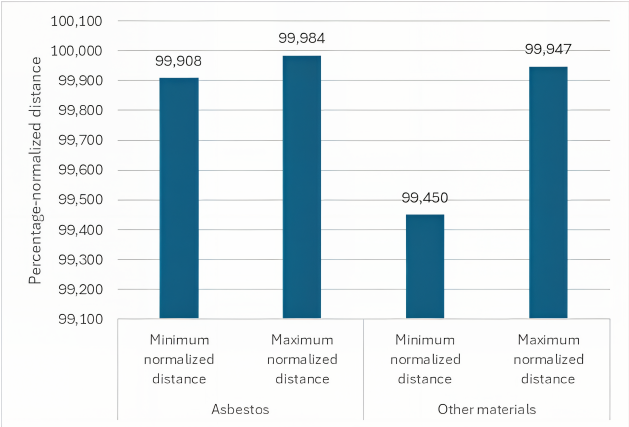

Figure 5: Evaluation of the method with asbestos and non-asbestos pixels with threshold at the median.

asbestos spectral signature and the Hamming distance to effectively differentiate asbestos pixels from pixels of other materials.

Taking this into account, the previous procedure was repeated by iterating through different thresholds, using as thresholds those corresponding to each of the 100 quantiles of the characteristic spectral signature or average pixel of asbestos-cement. In this way, Figure 6 presents only the quantiles that, through their thresholds and binarized signatures, achieved a positive difference between the minimum percentage-normalized Hamming distance with asbestos pixels and the maximum percentage-normalized Hamming distance with pixels of other materials.

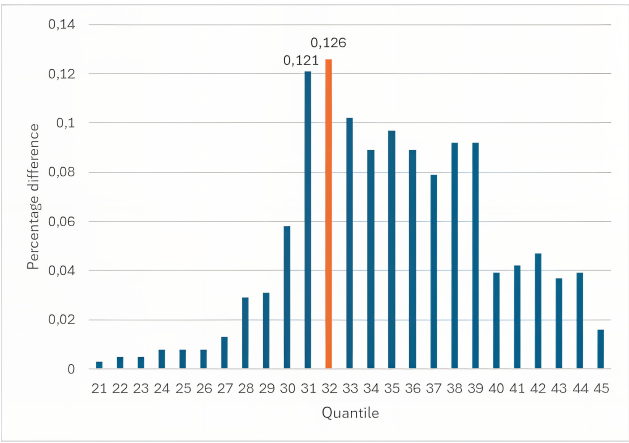

Figure 6: Percentage difference per quantile of the asbestos spectral signature.

According to the results presented in Figure 6, it can be observed that the greatest differences between the minimum percentage-normalized Hamming distance with asbestos pixels and the maximum percentage-normalized Hamming distance with pixels of other materials are obtained in the 31st and 32nd quantiles of the spectral signature, both exceeding a difference of 0.12. The 32nd quantile exhibits the highest difference, with a value of 0.126 and a threshold value of 0.115.

Thus, this threshold value resulted in a minimum Hamming percentage distance for detection of 99.939%, which was used for the implementation of the method on the complete reference image. In this way, the binarized spectral signature of the average or characteristic pixel of asbestos-cement, corresponding to the optimal threshold (0.115), is presented in Figure 7.

According to Figure 7, the binarized pixel of asbestos-cement transitions from 0 to 1 between band 100 and band 150, before returning to 0 after band 350. This behavior indicates a high reflectance range in the spectral region between these bands, suggesting a strong response at these wavelengths. The stability of the signal at 1 within this interval highlights the material's coherence in terms of its spectral properties, while the return to 0 after band 350 suggests a decrease in reflectance in those spectral regions.

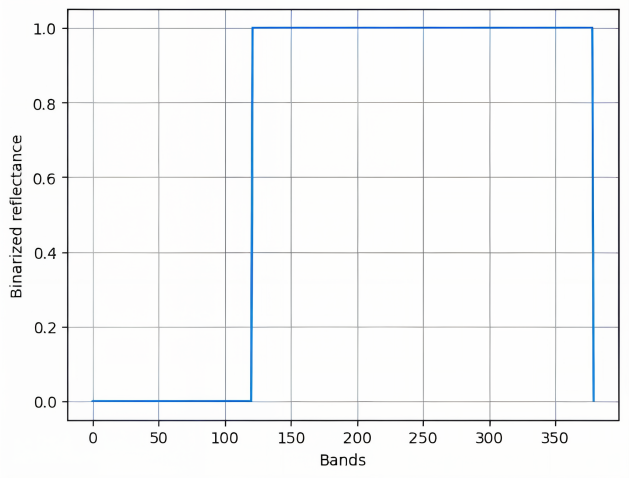

Figure 7: Binarized spectral signature corresponding to the optimal threshold.

Based on the binarized signature from Figure 7 and the minimum detection percentage obtained with this signature, the proposed method was applied to the complete reference image of the Manga neighborhood in the city of Cartagena. As shown in Figure 8, this implementation utilized the spectral and numpy libraries, with the detected asbestos-cement areas highlighted in blue.

It can be observed in Figure 8 that the digitize method from the numpy library was used to obtain the binarized spectral signature of both the average pixel and each pixel in the image. Likewise, array operations in numpy enabled the implementation of the normalized Hamming distance between the binarized spectral signatures of the average pixel and each pixel in the image. Similarly, it is worth mentioning that as a result of applying the proposed method to the complete hyperspectral image, it was determined that 9.63% of the pixels correspond to asbestos pixels. This percentage, along with the detected areas in the case study image, is highly useful for formulating strategic decisions by governmental authorities regarding the mitigation of asbestos-cement, considering the significant public health implications of this material.

```
#Threshold determination for the 32% quantile
umbral=np.asarray([cuar_prom[32]])
arr_copia=np.copy(arr)
tam=arr_norm.shape
cont=0
for i in range(tam[0]):
  for j in range(tam[1]):
    #Pixel i,j of the image
    pix=arr_norm[i][j]
    #Binarization of pixel i,j
    arr_bin = np.digitize(pix, umbral)
    #Calculation of the percentage-normalized Hamming distance
    dis_hamm_norm = np.sum(arr_bin != arr_bin_prom) / len(arr_bin)
    porc_dist=100-dis_hamm_norm
    #Selection of asbestos pixels
    if(porc_dist>=99.939):
      arr_copia[i][j]=150
      cont+=1
porc_asb=(cont/(tam[0]*tam[1]))*100
print(f"Abs Perc {porc_asb}")
```

```
Abs Perc 9.629208924949289
```

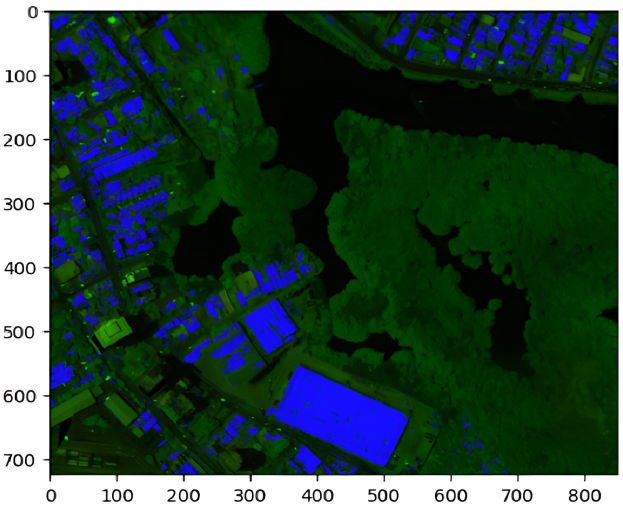

Figure 8: Implementation of the method on the case study image.

In order to evaluate the effectiveness of the proposed method compared to the correlation method, which has been widely used for material detection in hyperspectral images, the implementation of this method was carried out primarily using the spectral, scipy, and numpy libraries, as shown in Figure 9.

Based on the results obtained in Figure 9, it can be observed that the correlation method identified 9.79% of the pixels in the case study image as asbestos-cement. Compared to the proposed method, the correlation method detected only 0.16% more asbestos pixels, allowing us to conclude that the proposed method is as effective as the correlation method. In the same sense, to evaluate the computational efficiency of the proposed method relative to the correlation method, a 20×20 pixel region was selected, with each pixel containing 380 reflectance bands, and both methods were executed on this region for 25, 50, 75, and 100 repetitions. The processing times for each method are presented in Figure 10. It is worth mentioning that these results were obtained using Python's timeit library, which allows for measuring the processing time of a method across different executions.

```
[33] arr_copia=np.copy(arr)
     tam=arr_copia.shape
     cont_pix=0
     for i in range(tam[0]):
       for j in range(tam[1]):
         #Obtaining the pixel i,j of the image
         arr_temp=arr_norm[i][j]
         cont=np.count_nonzero(arr_temp)
         if(cont!=0):
           #Calculation of the correlation with respect to the average pixel
           corr=ssd.correlation(pix_prom, arr_temp)
           corr=corr/2
           #Obtaining the correlation percentage
           porc=np.abs(1-np.abs(corr))*100
           if(porc>=99.276):
             arr_copia[i][j]=150
             cont_pix+=1
     porc_pix_asb=(cont_pix/(tam[0]*tam[1]))*100
     print("Asb Perc", porc_pix_asb,"%")

     Asb Perc 9.791480730223123 %
```

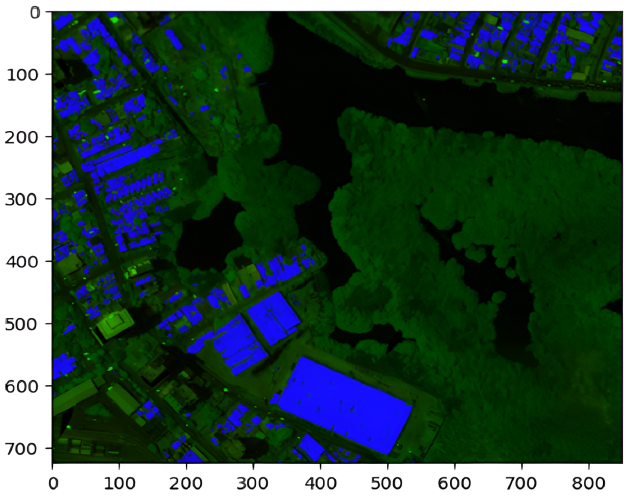

Figure 9: Implementation of the correlation method on the case study image.

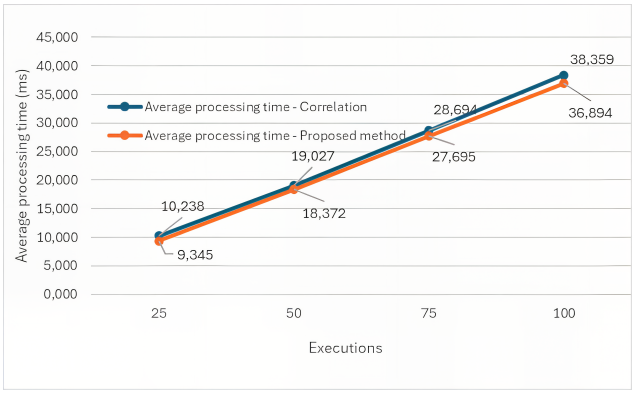

Figure 10: Average time per execution for each method.

According to the results presented in Figure 10, it can be observed that across all four execution groups, the correlation method exhibits slightly higher processing times compared to the proposed method. Consequently, when computing the overall average across different executions, it is determined that the correlation method is 1.05 times slower than the proposed method, meaning that the proposed method is 4.92% more efficient than the correlation method.

As a discussion, it is important to highlight that this article proposed a method for the detection of asbestos-cement in hyperspectral images as a contribution, utilizing the Hamming distance to compare the binarized spectral signature of asbestos with the binarized spectral signatures of other pixels. The results showed that this method is as effective as the correlation method while being 4.92% more efficient. Thus, this method emerges as a viable and competitive alternative for use in studies where the correlation method has been employed for material detection in hyperspectral images [23]. On the other hand, given the computational efficiency achieved by the proposed method, it also presents itself as a suitable option for asbestos detection in hyperspectral images compared to machine learning-based methods for detecting this material [14, 15]. Finally, since the implementation of the proposed method relied on open-source tools for both accessing the spectral information of the image and implementing and evaluating the method, this research is accessible for replication and extrapolation by universities and research centers for the detection of asbestos and other materials in hyperspectral images. This makes it a competitive alternative to proprietary tools currently used for material detection in remote sensing [28, 29, 30].

4 Conclusions and future work

- Given the need for efficient methods for material detection in hyperspectral images, this article proposed a new method for asbestos detection in hyperspectral images as a contribution, utilizing the Hamming distance to compare the binarized spectral signatures of the average asbestos pixel with those of the other pixels in the image. Considering that the proposed method proved to be as effective as the correlation method and slightly more efficient, it can be considered for integration into environmental monitoring systems based on hyperspectral images, given the necessity in these contexts to efficiently process large-volume images. To obtain the binarized spectral signature of asbestos-cement, the first step was to determine the conversion threshold, revealing that the threshold associated with the median exhibited overlap in distinguishing asbestos pixels from pixels of other materials. In this sense, by evaluating different thresholds associated with various quantiles of the spectral signature, it was determined that the 32% quantile allows for the maximum differentiation, enabling the detection of 9.63% of asbestos pixels in the implementation of the method. In this regard, depending on the type of material, it is essential to first identify the threshold that optimally enables the detection of each material.
- The results obtained in this study highlight two main contributions. First, the development of an efficient computational method for the detection of asbestos-cement coverings in hyperspectral images, based on the binarization of spectral signatures and Hamming distance. This approach allows reducing the dimensionality problem while maintaining an effective detection capability, which may favor the implementation of faster and scalable solutions in environmental mon-

itoring systems. On the other hand, the application of this method has a direct impact on public health, as it provides a useful tool for the identification of potentially hazardous materials in urban environments. Its implementation in remote sensing studies and government initiatives can facilitate the planning of asbestos mitigation and removal strategies in existing structures.

- Considering that the case study developed in this article allowed the proposed method to determine that the hyperspectral image of the Manga neighborhood in the city of Cartagena contains 9.63% asbestos pixels, with a 0.16% difference compared to the correlation method, this method demonstrates similar effectiveness. Consequently, it can be considered valid for integration and hybridization in material detection systems based on spectral images.
- From a computational perspective, the proposed method was evaluated alongside the correlation method through 25, 50, 75, and 100 repetitions on a 20×20 pixel region of the reference image, with each pixel containing 380 bands. The results showed that the correlation method is 1.05 times slower than the proposed method, meaning that the proposed method is 4.92% more efficient than the correlation method. This finding suggests that the proposed method can be considered for remote sensing applications where it is necessary to process large-scale hyperspectral images, enabling the generation of results in a shorter time compared to more sophisticated methods.
- This research demonstrated the relevance of using open-source tools for the processing and analysis of asbestos in hyperspectral images. In this way, the spectral library proved to be suitable for accessing the reflectance data of different pixels in the image, retrieving these data as numpy arrays. In turn, the numpy library was primarily useful for binarizing spectral signatures and implementing the normalized Hamming distance. Likewise, the scipy library facilitated the implementation of the correlation method, which was used to validate the computational efficiency of the proposed method. Furthermore, the matplotlib library enabled the generation of graphical representations of both conventional and binarized asbestos spectral signatures. In the same sense, the timeit library allowed for measuring the execution times of the methods under multiple repetitions. Thus, based on the libraries used, this work is intended to be replicable, scalable, and adaptable for the detection of different materials in hyperspectral images, serving as a competitive alternative to proprietary hyperspectral image processing tools.
- Finally, as a future research direction derived from this study, the effectiveness and efficiency of discretizing the spectral signature of asbestos-cement into more than two levels will be evaluated. Likewise, this method is intended to be extended for the detection of other materials of interest in the environmental domain, allowing for the assessment of its feasibility in the detection of vegetation and water bodies.

Funding
This article is considered a product within the framework of the project "Development of a comprehensive strategy to reduce the impact on public health and the environment due to the presence of asbestos in the territory of the department of Bolívar", funded by the General Royalties System of Colombia (SGR) and identified with code BPIN 2020000100366. This project was carried out by the University of Cartagena, Colombia, and the Asbestos-Free Colombia Foundation.

Acknowledgments
The authors acknowledge the Universidad de Cartagena and the General System of Royalties for the support provided in the development of this research.

Conflict of Interest
The authors declare no conflict of interest.

Authors' Contributions
Conceptualization: Gabriel Elías Chanchí-Golondrino, Manuel Alejandro Ospina-Alarcón; Methodology design: Manuel Saba; Data collection: Manuel Saba, Gabriel Elías Chanchí-Golondrino; Data analysis and interpretation: Gabriel Elías Chanchí-Golondrino, Manuel Alejandro Ospina-Alarcón, Manuel Saba; Writing and editing: Gabriel Elías Chanchí-Golondrino, Manuel Alejandro Ospina-Alarcón, Manuel Saba.

References

[1] J. Awange y J. Kiema, "Fundamentals of Remote Sensing", *Environmental Geoinformatics*, pp. 115-123, 2019. doi: 10.1007/978-3-030-03017-9_7.

[2] R. Navalgund, V. Jayaraman y P. S. Roy, "Remote sensing applications: An overview", *Current Science*, vol. 93, pp. 1747-1766, 2007.

[3] C. Nansen y N. Elliott, "Remote Sensing and Reflectance Profiling in Entomology", *Annual Review of Entomology*, vol. 61, no. 1, pp. 139-158, 2016. doi: 10.1146/annurevento-010715-023834.

[4] A. F. Jiménez-López, M. Jiménez-López y F. R. Jiménez-López, "Multispectral analysis of vegetation for remote sensing applications", *ITECKNE*, vol. 12, no. 2, 2015. doi: 10.15332/iteckne.v12i2.1242.

[5] A. A. Misra, "Remote Sensing Fundamentals", *Atlas of Structural Geological and Geomorphological Interpretation of Remote Sensing Images*, Wiley, pp. 7-14, 2022. doi: 10.1002/9781119813392.ch1.

[6] L. Gao y R. T. Smith, "Optical hyperspectral imaging in microscopy and spectroscopy - a review of data acquisition", *Journal of Biophotonics*, vol. 8, no. 6, pp. 441-456, 2015. doi: 10.1002/jbio.201400051.

[7] J. Burger y A. Gowen, "Data handling in hyperspectral image analysis", *Chemometrics and Intelligent Laboratory Systems*, vol. 108, no. 1, pp. 13-22, 2011. doi: 10.1016/j.chemolab.2011.04.001.

[8] H.-T. Lim y V. M. Murukeshan, "Spatial calibration and image processing requirements of an image fiber bundle based snapshot hyperspectral imaging probe: from raw data to datacube", en *Proceedings of SPIE*, 2017, p. 104491P. doi: 10.1117/12.2270739.

[9] R. Pizzolante y B. Carpentieri, "Hyperspectral Data: Efficient and Secure Transmission", *Algorithms*, vol. 10, no. 4, p. 132, 2017. doi: 10.3390/a10040132.

[10] M. J. Khan, H. S. Khan, A. Yousaf, K. Khurshid y A. Abbas, "Modern Trends in Hyperspectral Image Analysis: A Review", *IEEE Access*, vol. 6, pp. 14118-14129, 2018. doi: 10.1109/ACCESS.2018.2812999.

[11] Abhinav, A. J. S y S. Singh, "Spectral Signature Analysis of Land Sat TM Images for Improved Hyper Spectral Image Analysis", *Proceedings of the 2024 International Conference on Optimization Computing and Wireless Communication (ICOCWC)*, IEEE, pp. 1-6, 2024. doi: 10.1109/ICOCWC60930.2024.10470851.

[12] G. Bonifazi, G. Capobianco y S. Serranti, "Asbestos containing materials detection and classification by the use of hyperspectral imaging", *Journal of Hazardous Materials*, vol. 344, pp. 981-993, Feb. 2018.

[13] G. Bonifazi, G. Capobianco y S. Serranti, "Hyperspectral imaging applied to the identification and classification of asbestos fibers", en *2015 IEEE SENSORS*, IEEE, Nov. 2015, pp. 1-4. doi: 10.1109/ICSENS.2015.7370458.

[14] G. Bonifazi, G. Capobianco y S. Serranti, "Hyperspectral Imaging and Hierarchical PLS-DA Applied to Asbestos Recognition in Construction and Demolition Waste", *Applied Sciences*, vol. 9, no. 21, p. 4587, Oct. 2019. doi: 10.3390/app9214587.

[15] O. Trotta, G. Bonifazi, G. Capobianco y S. Serranti, "Detection of asbestos containing material in post-earthquake building waste through hyperspectral imaging and micro-X-ray fluorescence", *Detritus*, no. 21, pp. 27-34, 2022. doi: 10.31025/2611-4135/2022.17233.

[16] Y. Jeong, J. Yu, L. Wang, H. H. Huynh y H.-C. Kim, "Monitoring Asbestos Mine Remediation Using Airborne Hyperspectral Imaging System: A Case Study of Jefferson Lake Mine, US", *Remote Sensing*, vol. 14, no. 21, p. 5572, 2022. doi: 10.3390/rs14215572.

[17] W. Dong, C. Zhou, F. Wu, J. Wu, G. Shi y X. Li, "Model-Guided Deep Hyperspectral Image Super-Resolution", *IEEE Transactions on Image Processing*, vol. 30, pp. 5754-5768, 2021. doi: 10.1109/TIP.2021.3078058.

[18] B. Mohan y A. Porwal, "Hyperspectral Image Processing and Analysis", *Current Science*, vol. 108, pp. 833-841, 2015. doi: 10.18520/CS/V108/I5/833-841.

[19] M. E. Paoletti, J. M. Haut, N. S. Pereira, J. Plaza y A. Plaza, "Ghostnet for Hyperspectral Image Classification", *IEEE Transactions on Geoscience and Remote Sensing*, vol. 59, no. 12, pp. 10378-10393, 2021. doi: 10.1109/TGRS.2021.3050257.

[20] S. M. Schweizer y J. M. F. Moura, "Efficient detection in hyperspectral imagery", *IEEE Transactions on Image Processing*, vol. 10, no. 4, pp. 584-597, abr. 2001. doi: 10.1109/83.913593.

[21] R. Guerra, S. Lopez y R. Sarmiento, "A Computationally Efficient Algorithm for Fusing Multispectral and Hyperspectral Images," *IEEE Transactions on Geoscience and Remote Sensing*, vol. 54, no. 10, pp. 5712–5728, Oct. 2016. doi: 10.1109/TGRS.2016.2570433.

[22] A. Soccio, J. P. Barbosa y M. S. Reis, "A scalable approach for the efficient segmentation of hyperspectral images," *Chemometrics and Intelligent Laboratory Systems*, vol. 213, p. 104314, Jun. 2021.

[23] G. E. Chanchí Golondrino, M. A. Ospina Alarcón y M. Saba, "Vegetation Identification in Hyperspectral Images Using Distance/Correlation Metrics," *Atmosphere*, vol. 14, no. 7, p. 1148, Jul. 2023. doi: 10.3390/atmos14071148.

[24] E. F. Ávila Vélez,"Diseño de un modelo correlacional para cuantificar variables fisicoquímicas a partir de técnicas de espectroradiometría en cuerpos de agua. Caso de estudio río Cuja, Cundinamarca Colombia,"*Ciencia en Desarrollo*, vol. 15, no. 2, Oct. 2024.

[25] J. D. Caceres y A. N. Venkata, "Asbestos-associated pulmonary disease," *Current Opinion in Pulmonary Medicine*, vol. 29, no. 2, pp. 76-82, Mar. 2023.

[26] S. V. Jargin, "Asbestos-related Lung Diseases: A Brief Update," *Journal of Inflammatory Diseases*, vol. 26, no. 2, pp. 107–114, Jul. 2022. doi: 10.32598/JID.26.2.2.

[27] S. Klebe, V. Rathi y P. A. Russell, 'Lung cancer caused by asbestos: What a reporting pathologist needs to know," *Lung Cancer*, vol. 195, p. 107849, Sep. 2024.

[28] S. J. Hussein y Z. Fakhri Merzah, "Analysis of Hyperspectral Remote Sensing Images for Extraction Geological Rock Types Maps by Geospatial Techniques," *IOP Conference Series: Materials Science and Engineering*, vol. 901, no. 1, p. 012016, Aug. 2020. doi: 10.1088/1757-899X/901/1/012016.

[29] H. S. Jaber, "Classification of Hyperspectral Remote Sensing for Production Minerals Mapping Using Geological Map and Geomatics Techniques," *International Journal of Engineering & Technology*, 2018. doi: 10.14419/IJET.V7I4.20.26247.

[30] B. Bernacki y M. Phillips, "Standoff hyperspectral imaging of explosives residues using broadly tunable external cavity quantum cascade laser illumination," en *SPIE Defense, Security, and Sensing*, 2010.

[31] A. Korchevskiy and A. G. Wylie, "Asbestos Exposure, Lung Fiber Burden, and Mesothelioma Rates: Mechanistic Modelling for Risk Assessment," *Computational Toxicology*, vol. 24, p. 100249, 2022. doi: 10.1016/j.comtox.2022.100249.

[32] J. M. Ramada Rodilla, B. Calvo Cerrada, C. Serra Pujadas, G. L. Delclos, and F. G. Benavides, "Fiber burden and asbestos-related diseases: an umbrella review," *Gaceta Sanitaria*, vol. 36, no. 2, pp. 173–183, 2022. doi: 10.1016/j.gaceta.2021.04.001.

[33] P. V. Panou, M. Vyberg, C. Meristoudis, J. Hansen, M. Bøgsted, Ø. Omland, U. M. Weinreich, and O. D. Røe, "Non-occupational exposure to asbestos is the main cause of malignant mesothelioma in women in North Jutland, Denmark," *Scandinavian Journal of Work, Environment & Health*, vol. 45, no. 1, pp. 82–89, 2019. doi: 10.5271/sjweh.3756.